ACS Chemical Neuroscience

pubs.acs.org/chemneuro Research Article

Structural Rearrangement of the Serotonin Transporter Intracellular Gate Induced by Thr276 Phosphorylation

Matthew C. Chan, Erik Procko, and Diwakar Shukla*

Cite This: ACS Chem. Neurosci. 2022, 13, 933−945 Read Online

ACCESS | Metrics & More | Article Recommendations | Supporting Information

ABSTRACT: The reuptake of the neurotransmitter serotonin from the synaptic cleft by the serotonin transporter, SERT, is essential for proper neurological signaling. Biochemical studies have shown that Thr276 of transmembrane helix 5 is a site of PKG-mediated SERT phosphorylation, which has been proposed to shift the SERT conformational equilibria to promote inward-facing states, thus enhancing 5-HT transport. Recent structural and simulation studies have provided insights into the conformation transitions during substrate transport but have not shed light on SERT regulation via post-translational modifications. Using molecular dynamics simulations and Markov state models, we investigate how Thr276 phosphorylation impacts the SERT mechanism and its role in enhancing transporter stability and function. Our simulations show that Thr276 phosphorylation alters the hydrogen-bonding network involving residues on transmembrane helix 5. This in turn decreases the free energy barriers for SERT to transition to the inward-facing state, thus facilitating 5-HT import. The results provide atomistic insights into *in vivo* SERT regulation and can be extended to other pharmacologically important transporters in the solute carrier family.

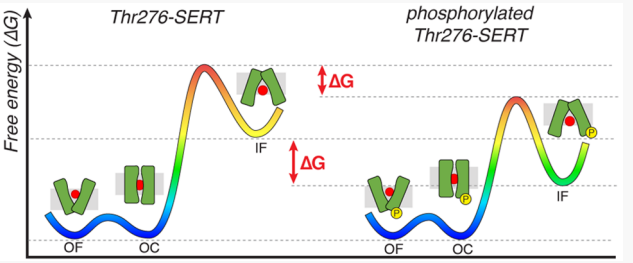

KEYWORDS: *Serotonin transporter, phosphorylation, molecular dynamics, Markov state models*

1. INTRODUCTION

The serotonin transporter (SERT, SLC6A4) is responsible for the reuptake of synaptic serotonin (5-hydroxytryptamine, 5-HT) from the synapse, thereby regulating serotonergic signaling in the brain and elsewhere in the body. SERT, as well as the dopamine transporter (DAT) and norephephine transporter (NET), are members of the sodium-coupled, chloride-dependent monoamine transporters in the neurotransmitter:sodium symporter (NSS) family or the solute carrier 6 (SLC6) family (1). Members of this family adopt an inverted pseudosymmetrical architecture consisting of 12 transmembrane (TM) helices commonly known as the LeuT fold[1,2] (Figure 1A). Transport of neurotransmitters across the neuronal membrane via the NSS family is facilitated by an alternating access mechanism, in which these transporters then undergo a series of conformational transitions from an outward-facing (OF) state, where the binding cavity is accessible from the extracellular side, to an occluded (OC) state, and finally an inward-facing (IF) state where the substrates are released into the neuron (Figure 1B,C).[3] Reverting back to the outward-facing state involves the efflux of potassium ions in some NSS transporters.[4]

In the body, SERT is regulated thorough numerous phosphorylation mechanisms that involve protein kinases, phosphatases, receptors, and substrates with implications for transporter expression, stability, trafficking, oligermization, and uptake activity.[5−7] Consequently, improper regulation of transporter function is associated with various physiological complications and psychiatric disorders.[8−11] Increased phosphorylation of SERT by protein-kinase-C-linked pathways is linked with increased SERT internalization and decreased 5-HT-transport activity.[12,13] Upregulation of SERT by protein kinase G (PKG) enhances expression and transport activity.[14−17] The psychostimulant drug amphetamine increases SERT phosphorylation,[13] and in DAT, amphetamine-induced phosphorylation of N-terminal residues exhibits a dopamine efflux function.[18,19] Among other transporters in the SLC family, phosphorylation heavily influences transporter function and trafficking and thus is a universal mechanism of regulating transporter activity.[20−23]

From a thermodynamics perspective, post-translational modifications (e.g., phosphorylation, glycosylation, lipidation) may alter the conformational free energy landscape, thus affecting protein stability and/or dynamics.[24,25] The use of molecular dynamics (MD) simulations not only provides an atomistic perspective of complex protein dynamics but also, upon sufficient sampling, may allow us to quantify the

Received: October 29, 2021
Accepted: February 22, 2022
Published: March 8, 2022

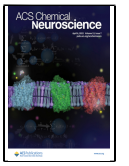

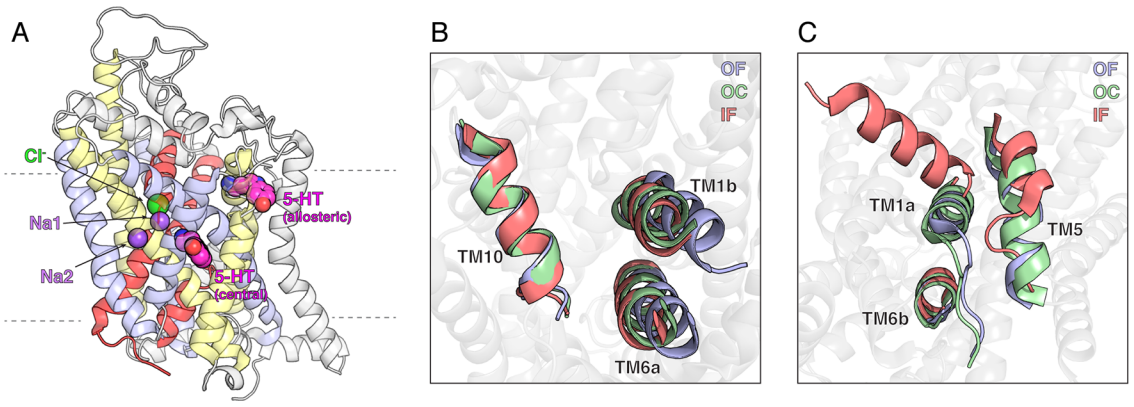

Figure 1. Architecture of the serotonin transporter, SERT. (A) Cryo-EM structure of SERT in the outward-facing conformation bound with serotonin (5-HT) in the central and allosteric sites (PDB: 7LIA). The sodium and chloride ions resolved in the crystal structure are shown as purple and green spheres, respectively. 5-HT bound in the allosteric and central sites is shown in magenta spheres. The twofold architecture of SERT is colored as follows: TM1 and TM6 in red, TM2−5 in light blue, TM7−10 in yellow, TM11−12 in gray. (B,C) SERT viewed from the extracellular plane (B) and intracellular plane (C) showing the conformational transitions of the gating helices involved in the transport process. The cryo-EM structures of SERT resolved in three states (OF (PDB: 7LIA): blue, OC (PDB: 7MGW): green, IF (PDB: 7LI9): salmon) are overlaid on the SERT-OF structure (gray). Structural alignment of the SERT conformational states was performed on all Cα atoms of the transporter.

thermodynamics of functional states and key transition barriers. For example, serine/threonine phosphorylation of protein kinases promotes active-like conformations by stabilizing the dynamics of flexible loops.[26−28] Alternatively, phosphorylation[27] and S-glutathionylation[29] of the plant kinase BAK1 alter the free energies where inactive states are favored over active-like states. Tyrosine nitration of an abscisic acid plant hormone receptor increases the free energy barriers for ligand binding, thereby preventing receptor activation.[30] As a final example, glycosylation of SH3 domains promotes their folded states due to the presence of bulky side chains that destabilize unfolded states.[31] Therefore, relating how post-translational modifications affect the protein dynamics and conformational free energy landscape is necessary to understand how protein function is regulated.

Potential SERT structural transitions to access the phosphorylation site for protein-kinase-mediated phosphorylation and protein−protein interactions have been extensively studied with the use of SERT substrates, kinase activators, and phosphatase inhibitors.[32,33] In 2007, Ramamoorthy et al. identified Thr276 of TM5 to be a site of PKG-mediated SERT phosphorylation (Figure 2A) and uncovered essential insights into the *in vivo* regulatory mechanisms of SERT trafficking and the transport function via post-translational modification.[17] It was later characterized through the binding of conformational selective inhibitors cocaine and ibogaine that the conformation of SERT controlled Thr276 phosphorylation to enhance 5-HT-transport activity.[34] Quantum dot studies conducted further correlated Thr276 phosphorylation with cholesterol depletion in midbrain neurons.[35] We have previously conducted large-scale MD simulations to characterize the serotonin import process in SERT. We showed how 5-HT binding in the orthosteric site reduces the free energy barriers for transition from the outward-facing to inward-facing states while also stabilizing the inward-facing state to promote substrate import.[36,37] In this current study, we aim to understand the molecular mechanism of Thr276 phosphorylation and its structural consequences on the conformational heterogeneity of SERT. We first performed MD simulations of SERT bound with inhibitors to provide atomistic details of Zhang et al.[34] Next, using our previously collected SERT data as a comparison,[36] we characterized the dynamics and structural stability of phosphorylated Thr276 SERT using Markov state models. To this extent, we collected over 600 μs of MD simulations data using the distributive computing platform Folding@Home[38] of phosphorylated Thr276 SERT. Our results show that Thr276 phosphorylation modulates SERT dynamics primarily through the rearrangement of intracellular hydrogen-bonding interactions. Consequently, the altered dynamics of the intracellular gating helices reduces the free energy barriers between occluded and inward-facing states and further stabilizes SERT in the inward-facing state for substrate import into the cell.

2. RESULTS AND DISCUSSION

2.1. Accessibility of the Thr276 Phosphorylation Site under Inhibitor Binding. Structural and computational studies on SERT have revealed that structural transitions from the outward-facing state to the inward-facing state of SERT are initiated by the binding of substrates in the orthosteric pocket, which triggers the movement of extracellular gating helices TM1b and TM6a toward the helical scaffold[36,39,40] (Figure 1B). The closure of the extracellular vestibule stabilizes the transporter to allow for solvation of the intracellular exit path and the formation of the inward-facing state. The conformation of the inward-facing state is notably associated with the outward motion of TM1a from the helical bundle and unwinding of the cytoplasmic base of TM5 to promote a solvent-exposed intracellular vestibule for substrate release[40−44] (Figure 1C). Multiple studies conducted by the Rudnick group investigated the reactivity of substituted cysteine residues with MTSEA (2-(aminoethyl)-methanethiosulfonate hydrobromide) as a measure of SERT accessibility and conformational transitions.[34,41,45−48] Of these studies, in 2016, Zhang et al. used cocaine and ibogaine to influence the conformational equilibria of outward-facing and inward-facing states and investigated the effects of Thr276 phosphorylation on the conformational dynamics and substrate transport mechanism.[34] They have identified PKG-mediated phosphorylation of Thr276 to occur more readily when SERT

https://doi.org/10.1021/acschemneuro.1c00714
ACS Chem. Neurosci. 2022, 13, 933−945

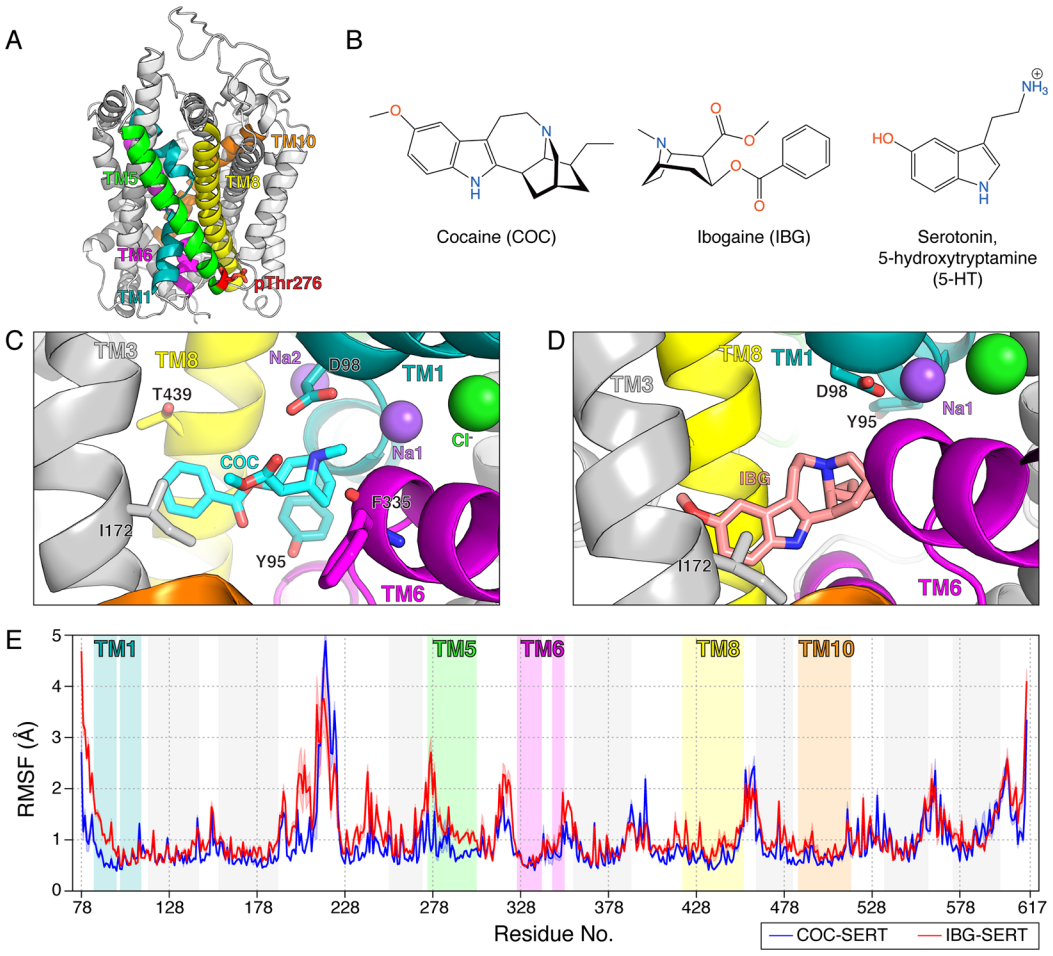

Figure 2. Dynamics of inhibitor-bound SERT. (A) A structural model of phosphorylated Thr276 SERT based on the outward-facing cryo-EM structure (PDB: 7LIA). Phosphorylated Thr276 is represented as red sticks. The SERT structure is represented as a cartoon with TM 1, 5, 6, 8, and 10 colored in teal, green, magenta, yellow, and orange, respectively. (B) Chemical structures for the conformational selective inhibitors cocaine and ibogaine and the endogenous substrate serotonin (5-HT). (C,D) MD snapshots of cocaine (C) and ibogaine (D) bound in the orthosteric site. TM helices 1, 5, 6, 8, and 10 colored in teal, green, magenta, yellow, and orange, respectively. (E) Root-mean-square fluctuation (RMSF) of cocaine-bound SERT (blue; in the OF state) and ibogaine-bound SERT (red; in the IF state). The calculated RMSF was averaged over five independent 250 ns simulations. Error bars represent the standard error among the five replicates. Residues spanning across transmembrane helices are shaded and colored as shown in panel A.

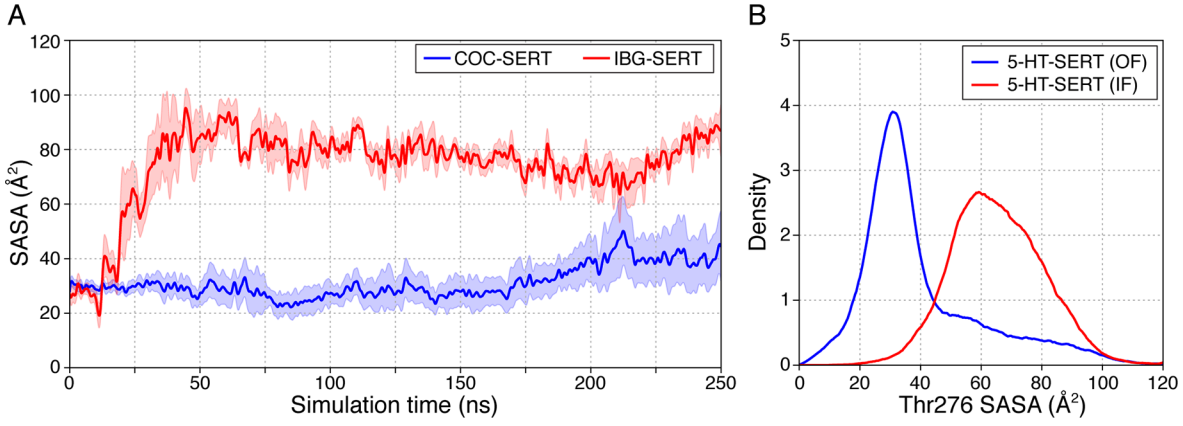

Figure 3. Accessibility of Thr276. (A) Calculated solvent-accessible surface area (SASA) of Thr276 for cocaine- (blue) and ibogaine-bound (red) SERT complexes. The calculated SASA was averaged over five independent 250 ns simulations. Standard error among the five replicates shown in respective shaded error bars. (B) Density distribution of Thr276 SASA from outward- and inward-facing states from SERT-5-HT import simulations.[36] Distribution of SASA was calculated based on 50 000 structures drawn from the respective energetic minima of the conformational free energy landscape. Calculation of SASA was implemented using the MDTraj python package[49] and a probe size of 1.4 Å.

https://doi.org/10.1021/acschemneuro.1c00714
ACS Chem. Neurosci. 2022, 13, 933−945

is bound with ibogaine as compared to cocaine. As ibogaine stabilizes SERT in an inward-facing state, this allows for TM5 to unwind and promote Thr276 phosphorylation. The cryo-EM structure of SERT bound with ibogaine would later be resolved to depict the unfolded structure of TM5.[40]

To provide an atomistic perspective of Zhang et al.'s observations, we performed MD simulations of SERT bound with inhibitors at the orthosteric site (Figure 2B). Cocaine docked in an outward-facing SERT crystal structure (PDB: 6AWO) or the ibogaine-complexed inward-facing cryo-EM SERT structure (PDB: 6DZZ) were used as the starting structures for simulations (Figure 2C,D). The proteins were embedded in a 1-palmitoyl-2-oleoyl-*sn*-glycero-3-phosphocholine (POPC) lipid bilayer and solvated with 150 mM NaCl. Five independent 250 ns long simulations for each SERT−inhibitor complex were performed. The cocaine−SERT and ibogaine−SERT complexes remained stable throughout the simulations with a backbone root-mean-square deviation (RMSD) of 1.8 ± 0.01 and 2.1 ± 0.2 Å, respectively (Figure S1).

The simulations show distinct structural characteristics of the respective SERT−inhibitor complexes. As expected, the fluctuations of TM1a in the intracellular vestibule are greater when SERT is in the ibogaine-bound inward-facing state versus the cocaine-bound outward-facing state (Figure 2E). Additionally, the fluctuations of extracellular loop (EL) 2 are more pronounced in simulations of the SERT−cocaine complex. This observation was also noted in our previous study illustrating the coupled dynamics of EL 2 and the opening and closure of the extracellular vestibule.[36] Most importantly, unwinding of the cytoplasmic base of TM5 in ibogaine-bound SERT promotes greater dynamics of the entire helix and intracellular loop (IL) 2 (Figures 2E, S1B).

The measurement of the solvent-accessible surface area (SASA) shows an increased solvent exposure of Thr276 in ibogaine-bound SERT simulations as compared to cocaine-bound SERT (Figures 3A, S1C). In the inward-facing SERT−ibogaine structure, the outward tilt of TM1a enables Tyr95 to interact with the backbone carbonyl of Thr276, while Tyr350 hydrogen-bonds with Gly273. These interactions initially stabilize the unfolded TM5, but after ∼50 ns in all five replicates, the hydrogen-bonding interactions break, and the unfolded TM5 region becomes exposed to the intracellular solvent (Figure S1D). Afterward, Thr276 remains exposed to the solvent, with an average SASA of 75 ± 0.18 Å^2 (mean ± SEM, over the last 100 ns) as compared to 36 ± 0.26 Å^2 in SERT−cocaine simulations. Furthermore, these observations are consistent with SASA calculations from our previous simulations with the endogenous substrate 5-HT (Figure 3B).[36] The binding of 5-HT enables a similar transition to the inward-facing state where unwinding of TM5 further allows Thr276 to be exposed to the cytoplasm. Overall, our observations of the accessibility of the Thr276 phosphorylation site are consistent with the findings presented by Zhang et al.[34]

2.2. Phosphorylation of Thr276 Alters the Conformational Free Energy Landscape. By projecting the electrostatic potential of the three-dimensional structure of SERT, we observed that phosphorylation of Thr276 affects the intracellular gate and neighboring residues (Figure S2). When closed, there is a positive surface charge at the intracellular gates of unphosphorylated Thr276−SERT, which for convenience we refer to as Thr276−SERT through the remainder of the manuscript. When Thr276 is phosphorylated, the electrostatics of residues surrounding the phosphorylation site become neutralized and thereby may alter the dynamics of the intracellular gate during occluded to inward-facing transitions. Given the proximity of Thr276 to the intracellular gating domain, we sought to understand how phosphorylation affects the intrinsic dynamics using MD simulations of phosphorylated Thr276 SERT (pThr276−SERT). To efficiently explore the conformational landscape, we seeded 2520 independent pThr276−SERT simulations to be conducted on Folding@Home.[38] The starting structures were selected from 18 macrostates of the Thr276−SERT simulations and Markov state model (MSM) obtained from our previous study (Figure S3).[36] An aggregated total of ∼630 μs of simulation data was collected and used to construct a MSM.

Projection of the MSM-weighted simulation data on the axes defined by the extracellular and intracellular gating residues quantifies the relative stability of SERT conformational states (Figure 4). In Thr276−SERT simulations, transitions from the occluded state to inward-facing state were rate-limiting for substrate import, with free energy barriers of ∼2 kcal/mol (Figure 4A).[36] Additionally, as compared to outward-facing and occluded states, the formation of inward-facing states in Thr276−SERT is relatively less stable.

The modification of Thr276 to phosphothreonine exhibits shifts in the free energy barriers of the conformational landscape. Transitions from outward-facing to occluded states retain relatively low free energy barriers. While outward-facing and occluded states remain stable with a relative free energy of ∼0−1 kcal/mol, the inward-facing state is further stabilized by ∼0.5−1 kcal/mol (Figure 4B). The transitions from occluded to inward-facing are further reduced by ∼0.5 kcal/mol as compared to Thr276−SERT (Figure 4C). As such, the increased stabilization of inward-facing states relative to outward-facing ones would further decrease the rate-limiting step of substrate import. Conformations in which both the extracellular and intracellular gates are open were also accessible in pThr276−SERT simualtions. We have previously characterized these conformations as an "hourglass"-like state, in which the permeation pathway is pinched at the Na2 site.[36] Likewise in Thr276−SERT, access to these hourglass like states is restricted with higher free energy barriers.

2.3. Rearrangement of the Intracellular Hydrogen-Bonding Network. The intracellular gate of SERT comprises a number of charged residues on TM1a, TM5, TM6b, and TM8 that form a hydrogen-bonding network to stabilize the transporter in outward-facing and occluded states (Figure 5A). These residues are conserved among other monoamine transporters as well as the NSS family. Several studies have highlighted the importance of the intracellular region in the NSS family and its role in the gating mechanism.[36,40,50−52] The binding of the substrates in the orthosteric site closes the extracellular vestibule, thereby initiating the breakage of these electrostatic interactions and promoting transitions to the inward-facing state where an intracellular exit pathway is formed between TM1a and TM5 (Figure 5C).

MD simulations of pThr276−SERT show that most of the interactions involving residues on the intracellular half are formed but with deviations of the distance distributions as compared to the Thr276−SERT simulations (Figure 5B,D). We observed that the phosphorylation of Thr276 disrupts the hydrogen-bonding interactions of residues on TM5, most notably Lys275, Lys279, and Trp282. The interactions are critical in stabilizing TM5 with TM1a, while the intracellular

https://doi.org/10.1021/acschemneuro.1c00714
ACS Chem. Neurosci. 2022, 13, 933−945

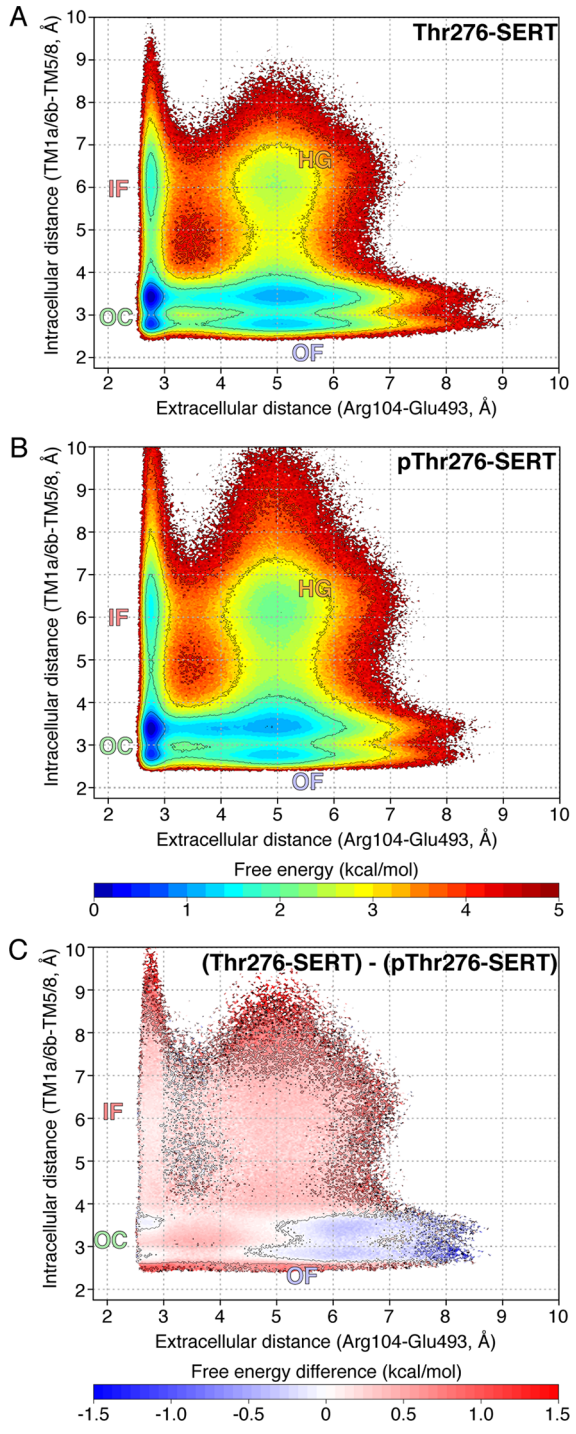

Figure 4. Phosphorylation of Thr276 alters the SERT conformational free energy landscape. (A,B) Conformational free energy landscapes for Thr276−SERT (A) and pThr276−SERT (B) projected on the coordinates defined by the extracellular and intracellular gating distances. Simulation data were reweighted by the Markov state model equilibrium probabilities. (C) Difference between the free energy landscapes of Thr276−SERT and pThr276−SERT projected on the same coordinates of the gating distances. Conformations in red have relatively lower free energy in pThr276−SERT. For the conformational landscapes shown, the extracellular gating distances were defined as the closest heavy atom between Arg104 and Glu493. Intracellular gating distances were calculated as the closest heavy atom between the groups of residues Val86−Ser91,Tyr350 (TM1a/TM6b) and Val199−Trp282,Glu444 (TM5/TM8). OF: outward-facing, OC: occluded, IF: inward-facing, HG: hourglass.

gate is closed. When comparing the occluded structures from simulations, the distances for pThr276−SERT intracellular residue pairs exhibit a broader distribution suggesting overall weaker interactions. For the Asp80−Lys275 pair, the distance between these residues increases in pThr276−SERT simulations, especially when in inward-facing states (Figures 5D, S2). The electrostatic interactions Arg79−Asp452, Glu78−Arg462, and Glu78−Lys275 are more prevalent in pThr276−SERT as compared to Thr276−SERT (Figure 5B,D). Given the increased flexibility of the N-terminal tail, gating residues on the N-terminus such as Glu78, Arg79, and Glu80 may compensate for weaker interactions of TM1a and TM5 when Thr276 is phosphorylated and allow stable outward-facing and occluded states for substrate binding.

The helical structure of TM5 is maintained by the hydrogen-bonding interactions between the side chains of Thr276 and Ser277 with the backbone carbonyl of Ser269 on TM4 and the side chain of Glu444, respectively (Figure 6A). Upon conformational transitions to the inward-facing state, these interactions are severed, resulting in the unwinding of the cytoplasmic base of TM5.[42] The addition of the phosphate to Thr276 not only presents a negative surface charge but also prevents Thr276 from being the hydrogen-bond donor. (Figure 6B) shows the projection of the simulation data on the metrics defined by the distance of residues involved in hydrogen-bond formation of TM5 versus the average helical content of TM5. The free energy landscapes indicate that the interaction of the Thr276 side chain and the backbone carbonyl of Ser296 is severed in pThr276−SERT and results in greater unfolding of TM5. Furthermore, in Thr276−SERT simulations, Ser277 forms alternate interactions with Ser269 and Glu444; however, in pThr276−SERT, Ser277 maintains its interaction with Ser269 but not with Glu444. This hydrogen-bond rearrangement in pThr276−SERT is a result of the outward bend of the pThr276 residue due to its larger and negatively charged side chain. As a result, TM5 is unable to maintain its helical structure and may consequently affect closure of the inward-facing state to complete the full transport cycle. Furthermore, the structural consequence of Thr276 phosphorylation results in nearby charged residues (Arg79, Lys272, and Lys275) to interact with the phosphate group of pThr276, thereby weakening the interactions of TM5 (Figure 6C). Due to the flexible nature of the N-terminus, Arg79, which typically interacts with Asp452, forms interactions with the Thr276 phosphate group. Furthermore, the adjacent residue Lys275 may also interact with the phosphate group. These additional interactions may destabilize the intracellular gates and decrease the free energy barriers for transition to the inward-facing state.

We note the Thr276 phosphorylation site is located near a conserved cholesterol binding site CHOL1, to be consistent with previous studies (Figure 7A).[53,54] Cholesterol has been extensively shown to directly influence the conformational equilibria of states; specifically, the depletion of cholesterol or mutations in the CHOL1 site promote inward-facing conformations.[54−56] Simulation of the related dopamine transporter shows that binding of cholesterol at CHOL1 sterically inhibits motions of TM1a and TM5 to stabilize the outward-facing conformation and prevents transitions to the inward-facing state.[53] Crystal structures of the *Drosophila* dopamine transporter[57] were resolved with a cholesterol hemisuccinate located at intracellular domains of TM2 and TM7 and noted as the CHOL2 site. A cholesterol hemi-

https://doi.org/10.1021/acschemneuro.1c00714
ACS Chem. Neurosci. 2022, 13, 933−945

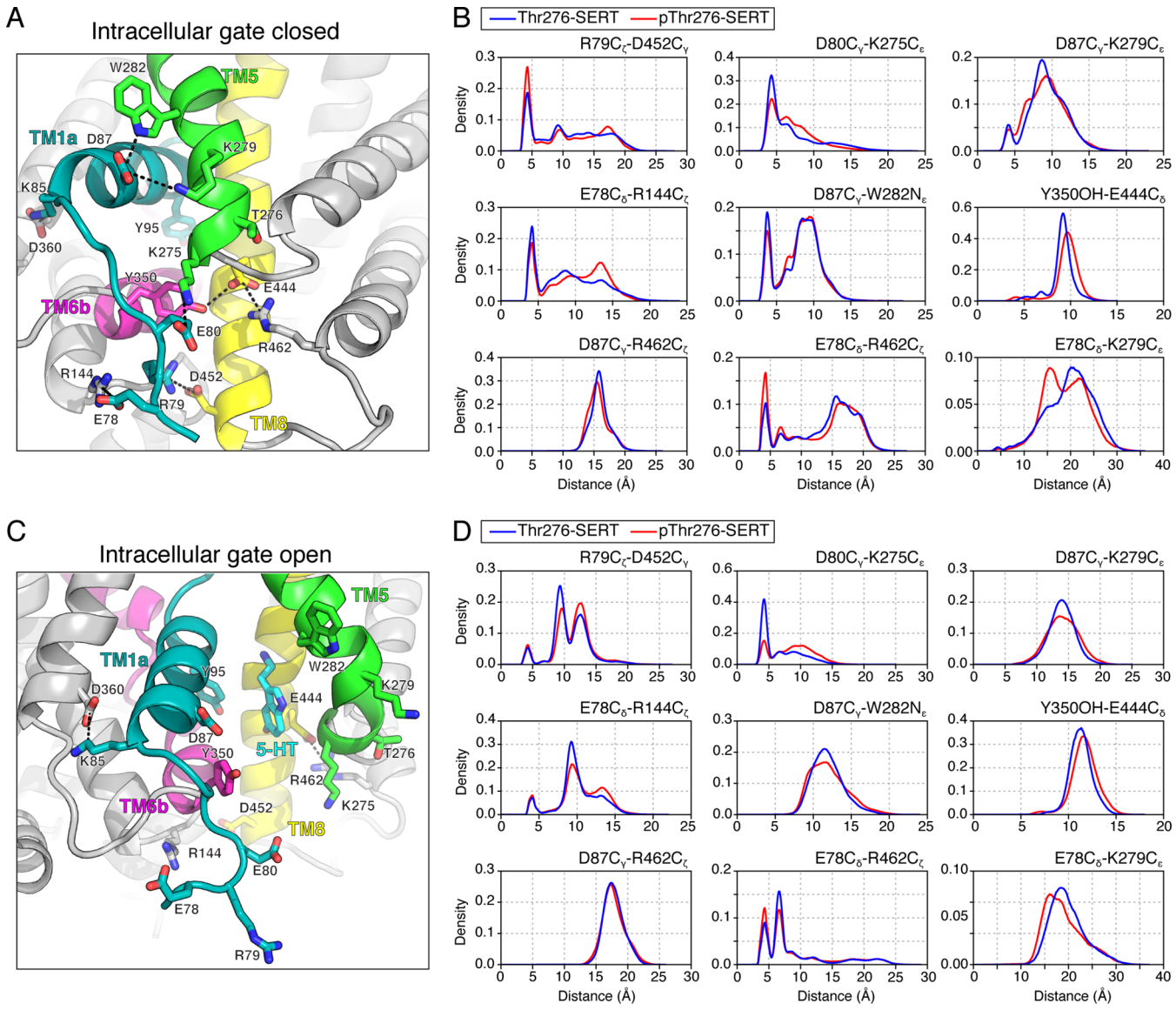

Figure 5. Rearrangement of the intracellular gating residues as a result of Thr276 phosphorylation. (A) MD snapshot of Thr276−SERT in the occluded and in the inward-facing states. Hydrogen-bonding pairs that contribute to the closure of the intracellular exit pathway are shown in sticks. (B) Distance distribution of residues involved in the closure of the intracellular vestibule. Distributions were based on 50 000 occluded structures drawn from the energetic minima of the conformational free energy landscape. Distances calculated from the Thr276−SERT MD simulations are represented in blue, while pThr276−SERT distances are calculated in red. (C,D) As in (A,B) but for the inward-facing state of SERT.

sucinate was also resolved in the serotonin transporter near TM12a.[58] As such, we sought to identify the extent of Thr276 phosphorylation on the dynamics of TM5 with cholesterol bound to SERT.

We conducted simulations of Thr276−SERT and pThr276−SERT in a POPC membrane with cholesterol initially bound to either site 1 (CHOL1) or site 2 (CHOL2) or both simultaneously (CHOL1/CHOL2). Thr276−SERT and pThr276−SERT systems with no cholesterol present in the membrane was used as controls for the respective systems. An outward-facing structure of SERT with serotonin, Na1, Na2, and Cl^- bound in their respective sites was used as the starting structure for these sets of simulations. A total of 10 replicates with different initial velocities were simulated for 1 μs each. We also simulated a SERT mutant, Thr276Asp (indicated as T276D−SERT), in the same manner as described. The mutation of Thr276Asp has been previously shown to increase 5-HT influx similar to that of the phosphorylated wild-type SERT.[17,59] While the phosphorylation site is removed, we hypothesized that the presence of an electronegative charge may alter the dynamics of the intracellular residues in a similar manner as pThr276.

For all SERT systems, the protein remained stable (backbone RMSD < 2 Å) throughout the 1 μs simulations (Figure S4A). We first assessed the stability of the cholesterol molecules in the cholesterol binding sites. Figure 7B shows the percentage of time cholesterol remained bound to each respective site across the 10 MD simulation replicates of CHOL1/CHOL2 simulations. We observed that the bound cholesterol molecule remains stable 50−60% of the total aggregated simulation time in the three SERT systems. Similarly observed in simulations of the dopamine transporter[53] and β2AR,[60] the decreased residence time of

https://doi.org/10.1021/acschemneuro.1c00714
ACS Chem. Neurosci. 2022, 13, 933−945

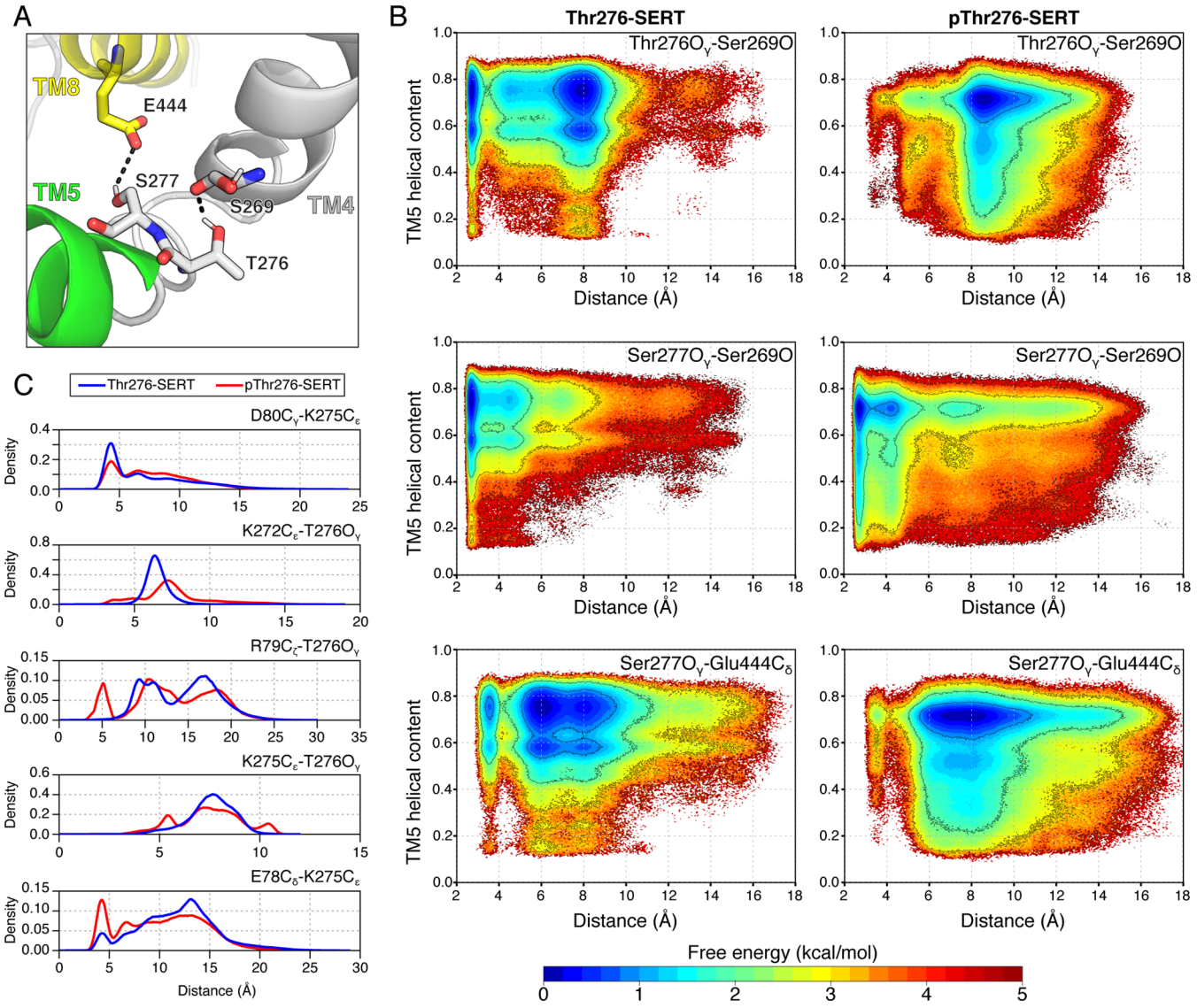

Figure 6. Thr276 phosphorylation further stabilizes the unwinding of TM5 during conformational transitions. (A) An outward-facing SERT crystal structure (PDB: 5I73) showing the hydrogen-bond arrangement to maintain the helical fold of TM5. The side chain of Thr276 interacts with the backbone carbonyl of Ser269 (TM4), while Ser277 hydrogen-bonds with Glu444. (B) Free energy landscapes comparing the helical content of TM5 and hydrogen bonds identified in panel (A). Helical content was measured for residues 273 to 280. Phosphorylation of Thr276 not only disrupts the hydrogen bonds formed by Ser269 but also further increases the unfolding of the cytoplasmic base of TM5. (C) Shifts in the distance distribution of hydrogen bonds involving residues neighboring Thr276. Distances calculated from the Thr276−SERT MSM are represented in blue, while the pThr276−SERT distances are represented in red.

cholesterol binding may be attributed to the reduced concentration of cholesterol in the membrane bulk.

The simulations suggest cholesterol binding does not significantly affect the solvation of Thr276 or the helical stability of TM5 (Figure 7C,D). In simulations of pThr276−SERT, either with cholesterol or without cholesterol, Thr276 remains exposed to the intracellular space, and TM5 has a greater propensity to unfold than Thr276−SERT. Simulations of the T276D mutant also show that Asp276 is more solvated than the wild-type (Figure S4B). Furthermore, the increased RMSD of the cytoplasmic base TM5 reflects the unfolding of the helix to promote structural rearrangements to the inward-facing state. In simulations in which cholesterol was initially bound to only CHOL1 or CHOL2, we observed similar trends to the simulations with both cholesterols simultaneously bound (Figure S5).

We further investigated if cholesterol binding would affect the intracellular hydrogen-bonding interactions, specifically interactions involving residues on TM5. Figure 8A shows the probability of hydrogen bonds formed that are present in the three studied systems, while Figure 8B,C shows hydrogen bonds formed uniquely to each system. The hydrogen-bonding network formed in the outward-facing conformation is maintained with and without the presence of cholesterol. Furthermore, the unique hydrogen-bonding interactions due to the introduction of the phosphate group from pThr276−SERT or the Asp side chain in T276D−SERT enable interactions of nearby Lys residues (Lys 272, Lys275, Lys279) to coordinate the unwinding of TM5 (Figure 8C,D). Overall, we find that direct binding of cholesterol does not significantly affect dynamics of phosphorylated Thr276 and the cytoplasmic base of TM5 when SERT is in the outward-facing state, but the new

https://doi.org/10.1021/acschemneuro.1c00714
ACS Chem. Neurosci. 2022, 13, 933−945

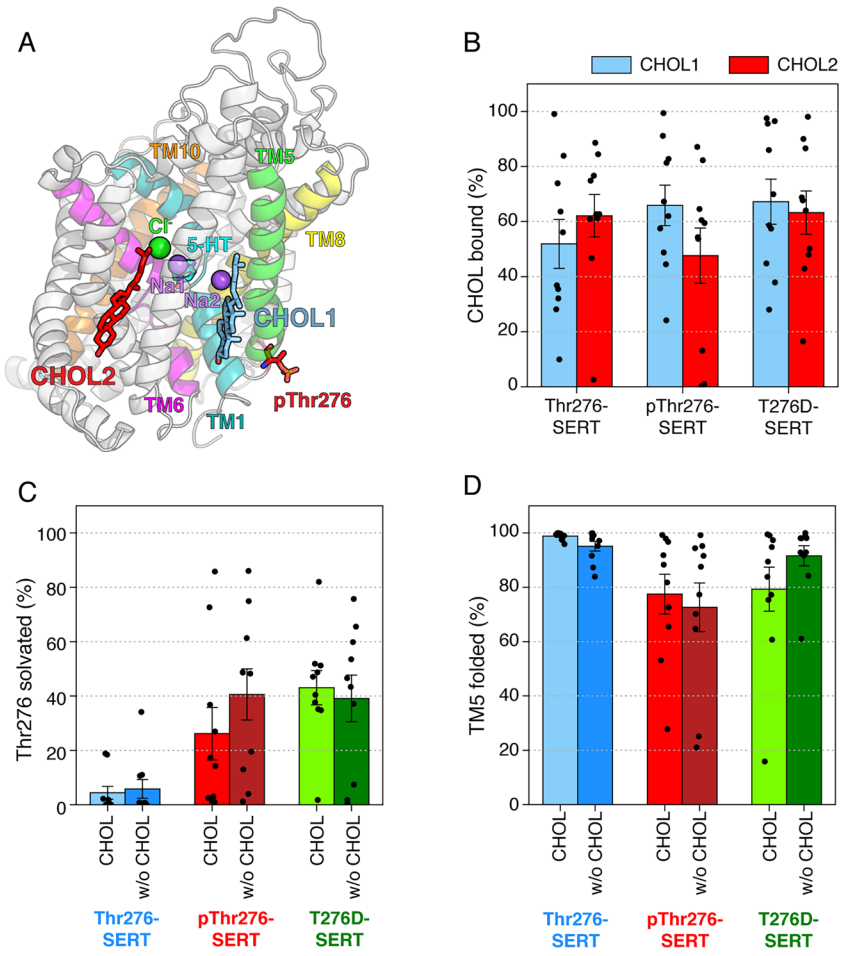

Figure 7. Effect of cholesterol binding on Thr276 solvation and TM5 helicity. (A) Structural model of pThr276−SERT based on PDB: 5I73 with cholesterol molecules bound based on the dopamine transporter PDB: 4XP1. (B) Stability of cholesterol in the binding site. The percentage of simulation frames in which cholesterol remained bound to the respective sites in simulations in which cholesterol was initially bound to both CHOL1 and CHOL2. A bound cholesterol was considered if the distance between the center of mass of cholesterol and respective binding site was less than 6 Å. (C) Percentage of simulation frames in which Thr276 was solvated. Averages are from simulations in which cholesterol was initially bound to both CHOL1 and CHOL2 (indicated as CHOL) and without cholesterol presented (w/o CHOL). Thr276 was considered solvated if the normalized solvent-accessible surface area (SASA) was greater than the normalized SASA of Thr276 in the inward-facing SERT structure PDB: 7ILA. To account for the difference in residue size, a normalized SASA was calculated as SASA/MaxSASA, in which MaxSASA is the SASA of a residue X in a fully extended Ala−X−Ala peptide. (D) Percentage of simulation frames in which TM5 was folded. TM5 was considered folded if the helicity was greater than 50%. For (B−D), the average percentage for 10 MD replicates is indicated as a black circle. Error bars represent standard error among the replicates.

interactions of nearby residues (Lys 272, Lys275, Lys279) with pThr276 or Thr276Asp enable the unwinding of TM5 to promote conformational transitions to the inward-facing state.

3. CONCLUSIONS

Understanding the molecular regulation of neurotransmitter transporters is vital for studying normal neurological function in the brain and developing therapeutics to treat various psychiatric disorders. The observations presented in this study provide an atomistic perspective into the mechanism of regulating SERT conformational dynamics by Thr276 phosphorylation. Using adaptive sampling and Markov state models to explore the SERT conformational space, we find that phosphorylated Thr276 results in the rearrangement of the intracellular hydrogen-bonding network, particularly residues involving TM5. These altered interactions consequently decrease the free energy barriers for occluded to inward-facing transitions and further stabilize the inward-facing state to allow for substrate release. We note that some of the altered interactions involving residues are located on the N-terminus domain. While the complete N-terminus domain was not modeled in our simulations, truncated SERT constructs with the cytoplasmic terminal domains removed have been shown to exhibit functional transport activity.[58,61,62] Nevertheless, it is possible the dynamics and interactions involving the phosphothreonine residue may differ in the full-length SERT promoter. Overall, the results obtained in this work alongside previously conducted experimental studies of Thr276 phosphorylation demonstrate how a phosphorylation event regulates SERT function through altering the conformational equilibria of outward-facing and inward-facing states.

Naturally occurring coding variants in human SERT have been shown to alter transporter regulation through changes in PKG/p38 mitogen-activated protein kinase-linked pathways.[63] The Ile425Val mutation has been identified in a subset of patients that exhibit obsessive-compulsive disorder and hyperactivity[64] and has been shown to enhance 5-HT transport due to dysregulated GMP regulation.[59,65] Furthermore, SERT

https://doi.org/10.1021/acschemneuro.1c00714
ACS Chem. Neurosci. 2022, 13, 933−945

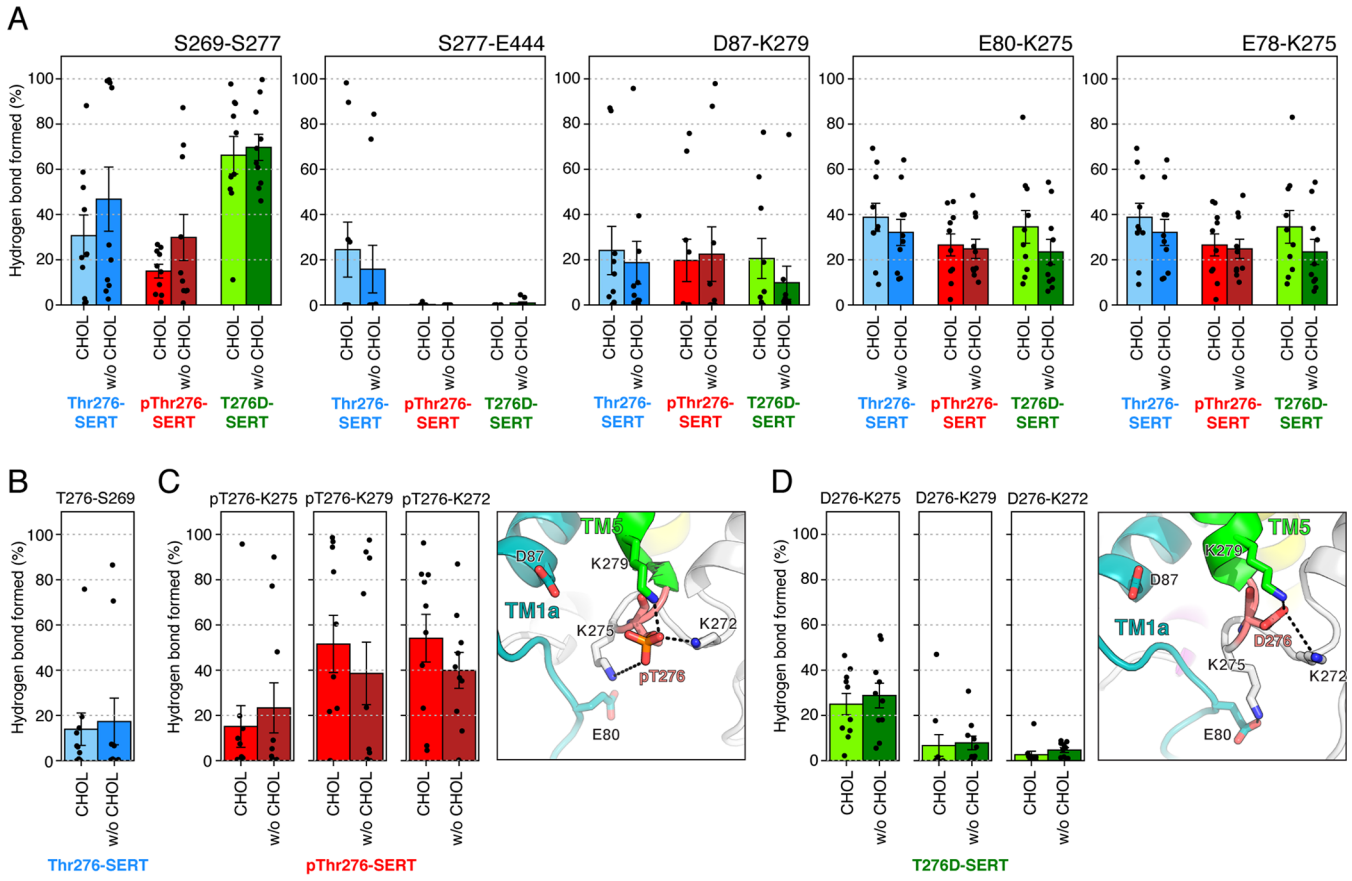

Figure 8. Effect of cholesterol binding on the intracellular hydrogen-bonding network. (A) Percentage of hydrogen bonds formed among the 10 MD simulations (1 μs long) of Thr276−SERT (blue), pThr276−SERT (red), and T276D−SERT (green) with cholesterol initially bound in sites 1 and 2 (indicated as CHOL) and without cholesterol present in the membrane (w/o CHOL). (B−D) Unique hydrogen bonds formed by the residue in position 276. (B) Percentage of Thr276−Ser269 formed in Thr276−SERT simulations. (C) Interactions of nearby lysine residues with the phosphate group of phosphothreonine. Representative MD snapshot of the lysine−phosphate interactions from pThr276−SERT simulations. (D) Interactions of nearby lysine residues with the Asp side chain. Representative MD snapshot of the lysine−aspartate interactions from T276D−SERT simulations. For all hydrogen-bond calculations, the respective hydrogen bond was considered formed based on a donor and acceptor atom distance cutoff of 3.5 Å. For all panels, the average percentage for 10 MD replicates is indicated as a black circle. Error bars represent standard error among the replicates.

containing the allelic variant Ala56 (normally Gly56 in wild-type) is subjected to hyperphosphorylation under basal conditions[66] and suggested to bias SERT in an outward-facing state.[67] The allelic variant Asn605 (normally Lys605 in wild-type) has been proposed to influence SERT in a similar manner as Ala56.[67] Other identified phosphorylation sites in SERT may affect overall transporter stability, including but not limited to protein trafficking, expression, and substrate uptake.[68,69]

Using molecular dynamics simulation and Markov state modeling, we present a mechanism in which phosphorylation of Thr276 modulates the intracellular hydrogen-bonding network to enhance 5-HT-transport activity. As this work focused on the conformational transitions associated with the substrate import process, that is, from outward-facing to inward-facing, how phosphorylated Thr276 affects SERT reverting to the outward-facing state and the transport of potassium remain unknown. The potassium binding site yet remains to be resolved, but it has been shown through biophysical experiments that potassium favors inward-facing-like states.[70,71] Furthermore, it is expected that the transitions from inward-facing to outward-facing conformations are rate-limiting for the complete SERT transport cycle.[72,73] From our simulations, we identified that Thr276 phosphorylation promotes the unwinding of the cytoplasmic base of TM5, a key structural requirement for the formation of the inward-facing state. Further studies may investigate how the kinetics of potassium efflux are altered when stimulated with PKG and if the hydrogen-bonding interactions formed due to phosphorylated Thr276 affect the closure of the inward-facing state.

4. METHODS

4.1. Overview of Simulations. We first simulated SERT bound with conformational selective inhibitors cocaine and ibogaine to examine the solvation of Thr276 as experimentally characterized by Zhang et al.[34] Cocaine docked in an outward-facing SERT structure or the ibogaine complexed inward-facing cryo-EM structure was used as the starting structure for the respective simulations. Five replicates of different initial velocities were simulated for 250 ns. Detailed methods on system construction and parametrization are presented in the Supplemental Methods and Table S1.

Secondly, to investigate the conformational dynamics involved in Thr276 phosphorylation, we seeded trajectories from the unphosphorylated Thr276−SERT Markov state model previously obtained in ref 36. Simulation details of pThr276−SERT are described in the subsequent section.

Finally, to elucidate the effects of cholesterol binding on the dynamics of pThr276−SERT, we performed three sets of simulations

https://doi.org/10.1021/acschemneuro.1c00714
ACS Chem. Neurosci. 2022, 13, 933−945

initiated from the outward-facing SERT crystal structure.[58] 5-HT, Na1, Na2, and Cl^- were initially bound. Cholesterol bound in either the CHOL1, CHOL2, both CHOL1 and CHOL2 sites, or not bound was simulated. A total of 10 replicates of different initial velocities were simulations for 1 μs each. We also simulated a Thr276Asp SERT mutant in the same protocol as described. A summary of cholesterol-bound SERT simulations is presented on Table S2. Further details of the system setup are described in the Supplemental Methods.

4.2. Phosphorylated Thr276−SERT Simulation on Folding@Home. Our previous study investigated the dynamics of the 5-HT import of Thr276−SERT.[36] These simulations consisted of one SERT protomer (residues 76−616) embedded in a POPC lipid bilayer, solvated with 150 mM NaCl and one 5-HT molecule in TIP3P water.[74] Terminal chains were capped with acetyl and methyl amide groups. Glu508 was modeled as the protonated form. A disulfide bridge was modeled between Cys200 and Cys209. The simulation data previously obtained was used to construct a Markov state model (MSM).

We clustered the unphosphorylated SERT Markov state model using the Perron-cluster cluster analysis+ (PCCA+) method to obtain starting structures for phosphorylated Thr276−SERT simulations. The PCCA+ algorithm constructs linear transformations of the eigenvectors of the transition matrix to obtain long-lived metastable states.[75] An initial 15 macrostates were assigned; however, the conformational sampling of the inward-facing conformation did not fully converge, and thus, we seeded structures from three macrostates centered around the Thr276−SERT inward-facing minima (Figure S3). A total of 70 structures from each macrostate were randomly sampled, totaling in 1260 unique conformations. For each structure, 2 replicates with different initial random velocities were created, totaling in 2520 independent MD simulations. Thr276 was modified to phosphothreonine (residue name TPO) using the tleap module of AmberTools. The phosphate group of phosphothreonine 276 was modeled as the doubly charged state given the pK_a of 6.30[76] and the neuron pH of 7.2.[77] Additional Na^+ ions were added to the simulation box to neutralize the system. Each system was prepared using OpenMM 7.4.2[78] and parametrized with an OpenMM ForceField using the Amber ff14SB[79] and GAFF force field.[80] Simulations were performed under periodic boundary conditions and NPT ensemble. The mass of hydrogen atoms and connected atoms were repartitioned according to Hopkins et al.[81] The Langevin integrator using a time step of 4 fs, temperature of 300 K, and collision rate of $\sqrt{2}$ ps^{-1} was used for Langevin dynamics. Pressure (1 atm) was maintained using the Monte Carlo Membrane Barostat with an update frequency of 100 steps. Nonbonded forces were calculated using the particle mesh Ewald method[82] with a 10 Å distance cutoff. The resulting OpenMM system and integrator file were serialized to XML format for Folding@Home.

Production simulations for the 2520 pThr276−SERT systems were conducted on Folding@Home using a simulation core based on OpenMM 7.4.2.[38,78] A maximum of 250 ns was collected for each system, totaling ∼630 μs of aggregated simulation data. pThr276−SERT simulations were conducted on Folding@Home from December 2020 to February 2021 and were conducted on various GPUs (Figure S6). Simulation snapshots were saved every 100 ps during production runs using mixed precision.

4.3. Markov State Modeling. MSMs are a statistical approach, in which the simulation data are discretized into kinetically relevant states and transition probabilities between each state are calculated. The resulting outcome of the MSM is a kinetic model, in which long-timescale protein dynamics can be characterized.[83,84] MSMs have been extensively employed to study protein folding, ligand binding, and conformational change processes.[85−87] However, there are only a few examples of the application of MSMs to membrane transporter proteins.[88−91] Here, we employ MSMs to compare the conformational ensemble of the phosphorylated and dephosophorylated SERT to obtain the thermodynamic and kinetic differences responsible for the shift in the conformational equilibrium upon phosphorylation.

All pThr276−SERT simulation data were used to construct a Markov state model (MSM) using the pyEMMA Python library.[92] To maintain consistency among the unphosphorylated SERT and phosphorylated SERT MSM, we used the same 16 residue−residue pair distances along the permeation pathway and z-components of the substrates as described in our previous study.[36] The number of clusters and time-independent components (tICs) were optimized by maximizing the VAMP1 score, or the sum of the eigenvalues of the transition matrix (Figure S7A). The phosphorylated SERT MSM was constructed using 500 clusters, 2 tICs, and a Markovian lag time of 12 ns (Figure S7B). The standard error of the free energy landscapes was calculated by bootstrapping with constructing the MSM with 80% of the trajectory set randomly selected for 500 independent samples (Figure S8). The constructed MSM was further validated using the Chapman-Kolmogorov test performed on five macrostates (Figure S9).

4.4. Trajectory Analysis. Trajectories were processed using the CPPTRAJ module of AmberTools[93] and MDTraj Python library[49] and visualized using Visual Molecular Dynamics (VMD)[94] and PyMOL (Schrödinger, LLC). The MSM-weighted simulation data were plotted on the coordinates of the extracellular and intracellular gating distances. Specifically, the extracellar distance was defined by the distance between the closest heavy atom between Arg104 and Glu493. Intracellular distance was calculated as the closest heavy atom distance between groups of residues Val86−Ser91, Tyr350 (TM1a, TM6b) and Val274−Trp282, Glu444 (TM5, TM8). Trajectory frames were assigned to an overall conformational state based on the free energy basin of the conformational landscape. Specifically, outward-facing conformations were defined if the extracellular gating distance was greater than 4.5 Å and intracellular gating distance was less than 4.0 Å, occluded used an extracellular distance less than 3.2 Å and intracellular distance less than 3.7 Å, and inward-facing used an extracellular distance less than 3.2 Å and intracellular distance greater than 5.5 Å. To calculate the distance distributions associated with a conformational state, 50 000 structures were randomly sampled from the free energy basin. In-house scripts utilizing the matplotlib Python library were used to generate plots and distributions.

■ ASSOCIATED CONTENT

Supporting Information

The Supporting Information is available free of charge at https://pubs.acs.org/doi/10.1021/acschemneuro.1c00714.

Description of system construction and methodology for inhibitor-bound SERT and cholesterol-bound SERT simulations; RMSD, SASA, helicity measurement of individual replicates of inhibitor-bound SERT simulations; electrostatic projection on the SERT surface; initial starting structure of pThr276−SERT simulations, comparison of cholesterol-bound system with CHOL1 or CHOL2 initially bound; Folding@Home statistics, hyperparameter optimization and validation of the MSM (PDF)

■ AUTHOR INFORMATION

Corresponding Author

Diwakar Shukla − *Department of Bioengineering, Department of Chemical and Biomolecular Engineering, Center for Biophysics and Quantitative Biology, Cancer Center at Illinois, and National Center for Supercomputing Applications, University of Illinois Urbana−Champaign, Urbana, Illinois 61801, United States;* orcid.org/0000-0003-4079-5381; Email: diwakar@illinois.edu

Authors

Matthew C. Chan − *Department of Chemical and Biomolecular Engineering, University of Illinois Urbana−Champaign, Urbana, Illinois 61801, United States;* orcid.org/0000-0002-9826-1983

https://doi.org/10.1021/acschemneuro.1c00714
ACS Chem. Neurosci. 2022, 13, 933−945

Erik Procko − *Department of Biochemistry, Center for Biophysics and Quantitative Biology, Neuroscience Program, and Cancer Center at Illinois, University of Illinois Urbana−Champaign, Urbana, Illinois 61801, United States*

Complete contact information is available at: https://pubs.acs.org/10.1021/acschemneuro.1c00714

Author Contributions

M.C.C. and D.S. designed the study. D.S. supervised the study. M.C.C. performed simulations. M.C.C., E.P., and D.S. analyzed data. M.C.C. wrote manuscript with input with E.P. and D.S.

Notes

The authors declare no competing financial interest.

Data availability: Trajectories of inhibitor-bound SERT and cholesterol-bound SERT with water and lipid molecules stripped are available free of charge on Zenodo at https://doi.org/10.5281/zenodo.5908025. Simulation data of phosThr276−SERT as well as full, unstripped trajectories of inhibitor-bound and cholesterol-bound SERT are available upon request, as the data set is over 700 GB in size. We do not enforce any limitation for how the data may be used once requested and shared.

■ ACKNOWLEDGMENTS

This work was supported by an NSF Early Career Award by NSF MCB 18-45606 to D.S. and R21 MH113155 from NIMH to E.P. This research is part of the Blue Waters sustained-petascale computing project, which is supported by the National Science Foundation (awards OCI-0725070 and ACI-1238993), the State of Illinois, and, as of December, 2019, the National Geospatial-Intelligence Agency. Blue Waters is a joint effort of the University of Illinois at Urbana−Champaign and its National Center for Supercomputing Applications. The authors thank Folding@Home donors for computational resources for this project. The authors also thank Zhiyu Zhao, Po-Chao Wen, and Emad Tajkhorshid from University of Illinois Urbana−Champaign for generously providing force field parameters for protonated ibogaine, and Jiming Chen and Jesse Horne for technical and illustrative discussions.

■ ABBREVIATIONS

SERT	serotonin transporter
DAT	dopamine transporter
NET	norephedrine transporter
NSS	neurotransmitter:sodium symporter
5-HT	5-hydroxytryptamine, serotonin
TM	transmembrane
OF	outward-facing
OC	occluded
IF	inward-facing
MSM	Markov state model
MD	molecular dynamics
RMSD	root-mean-square deviation
IL	intracellular loop
EL	extracellular loop
SASA	solvent-accessible surface area
RMSF	root-mean-square fluctuation
tIC	time-independent components
tICA	time-independent component analysis

■ REFERENCES

(1) Rudnick, G.; Krämer, R.; Blakely, R. D.; Murphy, D. L.; Verrey, F. The SLC6 transporters: perspectives on structure, functions, regulation, and models for transporter dysfunction. *Pflügers Archiv-European Journal of Physiology* **2014**, *466*, 25−42.

(2) Forrest, L. R. Structural symmetry in membrane proteins. *Annual Review of Biophysics* **2015**, *44*, 311−337.

(3) Mitchell, P. A general theory of membrane transport from studies of bacteria. *Nature* **1957**, *180*, 134−136.

(4) Nelson, P.; Rudnick, G. Coupling between platelet 5-hydroxytryptamine and potassium transport. *J. Biol. Chem.* **1979**, *254*, 10084−10089.

(5) Baudry, A.; Pietri, M.; Launay, J.-M.; Kellermann, O.; Schneider, B. Multifaceted Regulations of the Serotonin Transporter: Impact on Antidepressant Response. *Frontiers in Neuroscience* **2019**, *13*, 91.

(6) Ramamoorthy, S.; Shippenberg, T. S.; Jayanthi, L. D. Regulation of monoamine transporters: Role of transporter phosphorylation. *Pharmacology & therapeutics* **2011**, *129*, 220−238.

(7) Cooper, A.; Woulfe, D.; Kilic, F. Post-translational modifications of serotonin transporter. *Pharmacol. Res.* **2019**, *140*, 7−13.

(8) Ozaki, N.; Goldman, D.; Kaye, W.; Plotnicov, K.; Greenberg, B.; Lappalainen, J.; Rudnick, G.; Murphy, D. Serotonin transporter missense mutation associated with a complex neuropsychiatric phenotype. *Molecular psychiatry* **2003**, *8*, 933−936.

(9) Hansen, F. H.; Skjørringe, T.; et al. Missense dopamine transporter mutations associate with adult parkinsonism and ADHD. *J. Clin. Invest.* **2014**, *124*, 3107−3120.

(10) Kitzenmaier, A.; Schaefer, N.; Kasaragod, V. B.; Polster, T.; Hantschmann, R.; Schindelin, H.; Villmann, C. The P429L loss of function mutation of the human glycine transporter 2 associated with hyperekplexia. *European Journal of Neuroscience* **2019**, *50*, 3906−3920.

(11) Prasad, H. C.; Zhu, C.-B.; McCauley, J. L.; Samuvel, D. J.; Ramamoorthy, S.; Shelton, R. C.; Hewlett, W. A.; Sutcliffe, J. S.; Blakely, R. D. Human serotonin transporter variants display altered sensitivity to protein kinase G and p38 mitogen-activated protein kinase. *Proc. Natl. Acad. Sci. U. S. A.* **2005**, *102*, 11545−11550.

(12) Ramamoorthy, S.; Giovanetti, E.; Qian, Y.; Blakely, R. D. Phosphorylation and regulation of antidepressant-sensitive serotonin transporters. *J. Biol. Chem.* **1998**, *273*, 2458−2466.

(13) Ramamoorthy, S.; Blakely, R. D. Phosphorylation and sequestration of serotonin transporters differentially modulated by psychostimulants. *Science* **1999**, *285*, 763−766.

(14) Steiner, J. A.; Carneiro, A. M. D.; Wright, J.; Matthies, H. J.; Prasad, H. C.; Nicki, C. K.; Dostmann, W. R.; Buchanan, C. C.; Corbin, J. D.; Francis, S. H.; Blakely, R. D. cGMP-dependent protein kinase Ialpha associates with the antidepressant-sensitive serotonin transporter and dictates rapid modulation of serotonin uptake. *Molecular Brain* **2009**, *2*, 26.

(15) Miller, K. J.; Hoffman, B. J. Adenosine A3 receptors regulate serotonin transport via nitric oxide and cGMP. *J. Biol. Chem.* **1994**, *269*, 27351−27356.

(16) Launay, J. M.; Bondoux, D.; Oset-Gasque, M. J.; Emami, S.; Mutel, V.; Haimart, M.; Gespach, C. Increase of human platelet serotonin uptake by atypical histamine receptors. *American Journal of Physiology-Regulatory, Integrative and Comparative Physiology* **1994**, *266*, R526−R536.

(17) Ramamoorthy, S.; Samuvel, D. J.; Buck, E. R.; Rudnick, G.; Jayanthi, L. D. Phosphorylation of Threonine Residue 276 Is Required for Acute Regulation of Serotonin Transporter by Cyclic GMP. *J. Biol. Chem.* **2007**, *282*, 11639−11647.

(18) Khoshbouei, H.; Sen, N.; Guptaroy, B.; Johnson, L.; Lund, D.; Gnegy, M. E.; Galli, A.; Javitch, J. A. N-Terminal Phosphorylation of the Dopamine Transporter Is Required for Amphetamine-Induced Efflux. *PLoS Biology* **2004**, *2*, No. e78.

(19) Foster, J. D.; Yang, J.-W.; Moritz, A. E.; ChallaSivaKanaka, S.; Smith, M. A.; Holy, M.; Wilebski, K.; Sitte, H. H.; Vaughan, R. A. Dopamine transporter phosphorylation site threonine 53 regulates substrate reuptake and amphetamine-stimulated efflux. *J. Biol. Chem.* **2012**, *287*, 29702−29712.

(20) Seo, Y. A.; Kumara, R.; Wetli, H.; Wessling-Resnick, M. Regulation of divalent metal transporter-1 by serine phosphorylation. *Biochem. J.* **2016**, *473*, 4243−4254.
(21) Minematsu, T.; Giacomini, K. M. Interactions of Tyrosine Kinase Inhibitors with Organic Cation Transporters and Multidrug and Toxic Compound Extrusion Proteins. *Molecular Cancer Therapeutics* **2011**, *10*, 531−539.
(22) Annaba, F.; Sarwar, Z.; Gill, R. K.; Ghosh, A.; Saksena, S.; Borthakur, A.; Hecht, G. A.; Dudeja, P. K.; Alrefai, W. A. Enteropathogenic Escherichia coli inhibits ileal sodium-dependent bile acid transporter ASBT. *American Journal of Physiology-Gastrointestinal and Liver Physiology* **2012**, *302*, G1216−G1222.
(23) Sprowl, J. A.; Ong, S. S.; et al. A phosphotyrosine switch regulates organic cation transporters. *Nat. Commun.* **2016**, *7*, 10880.
(24) Millar, A. H.; Heazlewood, J. L.; Giglione, C.; Holdsworth, M. J.; Bachmair, A.; Schulze, W. X. The Scope, Functions, and Dynamics of Posttranslational Protein Modifications. *Annual Review of Plant Biology* **2019**, *70*, 119−151.
(25) Schönichen, A.; Webb, B. A.; Jacobson, M. P.; Barber, D. L. Considering Protonation as a Posttranslational Modification Regulating Protein Structure and Function. *Annual Review of Biophysics* **2013**, *42*, 289−314.
(26) Kuzmanic, A.; Sutto, L.; Saladino, G.; Nebreda, A. R.; Gervasio, F. L.; Orozco, M. Changes in the free-energy landscape of p38α MAP kinase through its canonical activation and binding events as studied by enhanced molecular dynamics simulations. *eLife* **2017**, *6*, e22175.
(27) Moffett, A. S.; Shukla, D. Structural Consequences of Multisite Phosphorylation in the BAK1 Kinase Domain. *Biophys. J.* **2020**, *118*, 698−707.
(28) Jonniya, N. A.; Sk, M. F.; Kar, P. Investigating Phosphorylation-Induced Conformational Changes in WNK1 Kinase by Molecular Dynamics Simulations. *ACS Omega* **2019**, *4*, 17404−17416.
(29) Moffett, A. S.; Bender, K. W.; Huber, S. C.; Shukla, D. Allosteric Control of a Plant Receptor Kinase through S-Glutathionylation. *Biophys. J.* **2017**, *113*, 2354−2363.
(30) Shukla, S.; Zhao, C.; Shukla, D. Dewetting controls plant hormone perception and initiation of drought resistance signaling. *Structure* **2019**, *27*, 692−702.
(31) Shental-Bechor, D.; Levy, Y. Effect of glycosylation on protein folding: a close look at thermodynamic stabilization. *Proc. Natl. Acad. Sci. U. S. A.* **2008**, *105*, 8256−8261.
(32) Ramamoorthy, S.; Blakely, R. D. Phosphorylation and Sequestration of Serotonin Transporters Differentially Modulated by Psychostimulants. *Science* **1999**, *285*, 763−766.
(33) Ramamoorthy, S.; Giovanetti, E.; Qian, Y.; Blakely, R. D. Phosphorylation and Regulation of Antidepressant-sensitive Serotonin Transporters. *J. Biol. Chem.* **1998**, *273*, 2458−2466.
(34) Zhang, Y.-W.; Turk, B. E.; Rudnick, G. Control of serotonin transporter phosphorylation by conformational state. *Proc. Natl. Acad. Sci. U. S. A.* **2016**, *113*, E2776−E2783.
(35) Bailey, D. M.; Catron, M. A.; Kovtun, O.; Macdonald, R. L.; Zhang, Q.; Rosenthal, S. J. Single quantum dot tracking reveals serotonin transporter diffusion dynamics are correlated with cholesterol-sensitive threonine 276 phosphorylation status in primary midbrain neurons. *ACS chemical neuroscience* **2018**, *9*, 2534−2541.
(36) Chan, M. C.; Selvam, B.; Young, H. J.; Procko, E.; Shukla, D. The substrate import mechanism of the human serotonin transporter. *Biophysical Journal* **2022**, *121*, 715−730.
(37) Young, H. J.; Chan, M.; Selvam, B.; Szymanski, S. K.; Shukla, D.; Procko, E. Deep Mutagenesis of a Transporter for Uptake of a Non-Native Substrate Identifies Conformationally Dynamic Regions. *bioRxiv*, 2021. https://www.biorxiv.org/content/10.1101/2021.04.19.440442v1.
(38) Shirts, M.; Pande, V. S. Screen savers of the world unite. *Science* **2000**, *290*, 1903−1904.
(39) Koldsø, H.; Noer, P.; Grouleff, J.; Autzen, H. E.; Sinning, S.; Schiøtt, B. Unbiased Simulations Reveal the Inward-Facing Conformation of the Human Serotonin Transporter and Na+ Ion Release. *PLoS Computational Biology* **2011**, *7*, No. e1002246.
(40) Coleman, J. A.; Yang, D.; Zhao, Z.; Wen, P.-C.; Yoshioka, C.; Tajkhorshid, E.; Gouaux, E. Serotonin transporter−ibogaine complexes illuminate mechanisms of inhibition and transport. *Nature* **2019**, *569*, 141−145.
(41) Zhang, Y.-W.; Rudnick, G. The cytoplasmic substrate permeation pathway of serotonin transporter. *J. Biol. Chem.* **2006**, *281*, 36213−36220.
(42) Malinauskaite, L.; Quick, M.; Reinhard, L.; Lyons, J. A.; Yano, H.; Javitch, J. A.; Nissen, P. A mechanism for intracellular release of Na+ by neurotransmitter/sodium symporters. *Nature Structural & Molecular Biology* **2014**, *21*, 1006−1012.
(43) Merkle, P. S.; Gotfryd, K.; Cuendet, M. A.; Leth-Espensen, K. Z.; Gether, U.; Loland, C. J.; Rand, K. D. Substrate-modulated unwinding of transmembrane helices in the NSS transporter LeuT. *Science Advances* **2018**, *4*, No. eaar6179.
(44) Krishnamurthy, H.; Gouaux, E. X-ray structures of LeuT in substrate-free outward-open and apo inward-open states. *Nature* **2012**, *481*, 469−474.
(45) Androutsellis-Theotokis, A.; Rudnick, G. Accessibility and conformational coupling in serotonin transporter predicted internal domains. *J. Neurosci.* **2002**, *22*, 8370−8378.
(46) Zhang, Y.-W.; Rudnick, G. Cysteine-scanning mutagenesis of serotonin transporter intracellular loop 2 suggests an α-helical conformation. *J. Biol. Chem.* **2005**, *280*, 30807−30813.
(47) Jacobs, M. T.; Zhang, Y.-W.; Campbell, S. D.; Rudnick, G. Ibogaine, a noncompetitive inhibitor of serotonin transport, acts by stabilizing the cytoplasm-facing state of the transporter. *J. Biol. Chem.* **2007**, *282*, 29441−29447.
(48) Zhang, Y.-W.; Tavoulari, S.; Sinning, S.; Aleksandrova, A. A.; Forrest, L. R.; Rudnick, G. Structural elements required for coupling ion and substrate transport in the neurotransmitter transporter homolog LeuT. *Proc. Natl. Acad. Sci. U. S. A.* **2018**, *115*, E8854−E8862.
(49) McGibbon, R.; Beauchamp, K.; Harrigan, M.; Klein, C.; Swails, J.; Hernández, C.; Schwantes, C.; Wang, L.-P.; Lane, T.; Pande, V. MDTraj: A Modern Open Library for the Analysis of Molecular Dynamics Trajectories. *Biophys. J.* **2015**, *109*, 1528−1532.
(50) Zhao, Y.; Terry, D. S.; Shi, L.; Quick, M.; Weinstein, H.; Blanchard, S. C.; Javitch, J. A. Substrate-modulated gating dynamics in a Na+-coupled neurotransmitter transporter homologue. *Nature* **2011**, *474*, 109−113.
(51) Cheng, M. H.; Bahar, I. Molecular mechanism of dopamine transport by human dopamine transporter. *Structure* **2015**, *23*, 2171−2181.
(52) Dehnes, Y.; Shan, J.; Beuming, T.; Shi, L.; Weinstein, H.; Javitch, J. A. Conformational changes in dopamine transporter intracellular regions upon cocaine binding and dopamine translocation. *Neurochemistry international* **2014**, *73*, 4−15.
(53) Zeppelin, T.; Ladefoged, L. K.; Sinning, S.; Periole, X.; Schiøtt, B. A direct interaction of cholesterol with the dopamine transporter prevents its out-to-inward transition. *PLOS Computational Biology* **2018**, *14*, No. e1005907.
(54) Laursen, L.; Severinsen, K.; Kristensen, K. B.; Periole, X.; Overby, M.; Müller, H. K.; Schiøtt, B.; Sinning, S. Cholesterol binding to a conserved site modulates the conformation, pharmacology, and transport kinetics of the human serotonin transporter. *J. Biol. Chem.* **2018**, *293*, 3510−3523.
(55) Bjerregaard, H.; Severinsen, K.; Said, S.; Wiborg, O.; Sinning, S. A Dualistic Conformational Response to Substrate Binding in the Human Serotonin Transporter Reveals a High Affinity State for Serotonin. *J. Biol. Chem.* **2015**, *290*, 7747−7755.
(56) Scanlon, S. M.; Williams, D. C.; Schloss, P. Membrane Cholesterol Modulates Serotonin Transporter Activity. *Biochemistry* **2001**, *40*, 10507−10513.
(57) Penmatsa, A.; Wang, K. H.; Gouaux, E. X-ray structure of dopamine transporter elucidates antidepressant mechanism. *Nature* **2013**, *503*, 85−90.

(58) Coleman, J. A.; Green, E. M.; Gouaux, E. X-ray structures and mechanism of the human serotonin transporter. *Nature* **2016**, *532*, 334−339.
(59) Zhang, Y.-W.; Gesmonde, J.; Ramamoorthy, S.; Rudnick, G. Serotonin Transporter Phosphorylation by cGMP-Dependent Protein Kinase Is Altered by a Mutation Associated with Obsessive Compulsive Disorder. *J. Neurosci.* **2007**, *27*, 10878−10886.
(60) Manna, M.; Niemelä, M.; Tynkkynen, J.; Javanainen, M.; Kulig, W.; Müller, D. J.; Rog, T.; Vattulainen, I. Mechanism of allosteric regulation of β2-adrenergic receptor by cholesterol. *eLife* **2016**, *5*, No. e18432.
(61) Sucic, S.; Dallinger, S.; Zdrazil, B.; Weissensteiner, R.; Jørgensen, T. N.; Holy, M.; Kudlacek, O.; Seidel, S.; Cha, J. H.; Gether, U.; Newman, A. H.; Ecker, G. F.; Freissmuth, M.; Sitte, H. H. The N Terminus of Monoamine Transporters Is a Lever Required for the Action of Amphetamines. *J. Biol. Chem.* **2010**, *285*, 10924−10938.
(62) Kern, C.; Erdem, F. A.; El-Kasaby, A.; Sandtner, W.; Freissmuth, M.; Sucic, S. The N Terminus Specifies the Switch between Transport Modes of the Human Serotonin Transporter. *J. Biol. Chem.* **2017**, *292*, 3603−3613.
(63) Prasad, H. C.; Zhu, C.-B.; McCauley, J. L.; Samuvel, D. J.; Ramamoorthy, S.; Shelton, R. C.; Hewlett, W. A.; Sutcliffe, J. S.; Blakely, R. D. Human serotonin transporter variants display altered sensitivity to protein kinase G and p38 mitogen-activated protein kinase. *Proc. Natl. Acad. Sci. U. S. A.* **2005**, *102*, 11545−11550.
(64) Ozaki, N.; Goldman, D.; Kaye, W. H.; Plotnicov, K.; Greenberg, B. D.; Lappalainen, J.; Rudnick, G.; Murphy, D. L. Serotonin transporter missense mutation associated with a complex neuropsychiatric phenotype. *Molecular Psychiatry* **2003**, *8*, 933−936.
(65) Kilic, F.; Murphy, D. L.; Rudnick, G. A Human Serotonin Transporter Mutation Causes Constitutive Activation of Transport Activity. *Mol. Pharmacol.* **2003**, *64*, 440−446.
(66) Veenstra-VanderWeele, J.; Muller, C. L.; et al. Autism gene variant causes hyperserotonemia, serotonin receptor hypersensitivity, social impairment and repetitive behavior. *Proc. Natl. Acad. Sci. U. S. A.* **2012**, *109*, 5469−5474.
(67) Quinlan, M. A.; Krout, D.; Katamish, R. M.; Robson, M. J.; Nettesheim, C.; Gresch, P. J.; Mash, D. C.; Henry, L. K.; Blakely, R. D. Human Serotonin Transporter Coding Variation Establishes Conformational Bias with Functional Consequences. *ACS Chem. Neurosci.* **2019**, *10*, 3249−3260.
(68) Annamalai, B.; Mannangatti, P.; Arapulisamy, O.; Shippenberg, T. S.; Jayanthi, L. D.; Ramamoorthy, S. Tyrosine Phosphorylation of the Human Serotonin Transporter: A Role in the Transporter Stability and Function. *Mol. Pharmacol.* **2012**, *81*, 73−85.
(69) Sørensen, L.; Strømgaard, K.; Kristensen, A. S. Characterization of Intracellular Regions in the Human Serotonin Transporter for Phosphorylation Sites. *ACS Chem. Biol.* **2014**, *9*, 935−944.
(70) Möller, I. R.; Slivacka, M.; Nielsen, A. K.; Rasmussen, S. G.; Gether, U.; Loland, C. J.; Rand, K. D. Conformational dynamics of the human serotonin transporter during substrate and drug binding. *Nat. Commun.* **2019**, *10*, 1687.
(71) Yang, D.; Gouaux, E. Illumination of serotonin transporter mechanism and role of the allosteric site. *Science Advances* **2021**, *7*, No. eabl3857.
(72) Schicker, K.; Uzelac, Z.; Gesmonde, J.; Bulling, S.; Stockner, T.; Freissmuth, M.; Boehm, S.; Rudnick, G.; Sitte, H. H.; Sandtner, W. Unifying Concept of Serotonin Transporter-associated Currents. *J. Biol. Chem.* **2012**, *287*, 438−445.
(73) Hasenhuetl, P. S.; Freissmuth, M.; Sandtner, W. Electrogenic Binding of Intracellular Cations Defines a Kinetic Decision Point in the Transport Cycle of the Human Serotonin Transporter. *J. Biol. Chem.* **2016**, *291*, 25864−25876.
(74) Jorgensen, W. L.; Chandrasekhar, J.; Madura, J. D.; Impey, R. W.; Klein, M. L. Comparison of simple potential functions for simulating liquid water. *J. Chem. Phys.* **1983**, *79*, 926−935.
(75) Röblitz, S.; Weber, M. Fuzzy spectral clustering by PCCA+: application to Markov state models and data classification. *Advances in Data Analysis and Classification* **2013**, *7*, 147−179.
(76) Bienkiewicz, E. A.; Lumb, K. J. Random-coil chemical shifts of phosphorylated amino acids. *Journal of Biomolecular NMR* **1999**, *15*, 203−206.
(77) Raley-Susman, K. M.; Cragoe, E. J.; Sapolsky, R. M.; Kopito, R. R. Regulation of intracellular pH in cultured hippocampal neurons by an amiloride-insensitive Na+/H+ exchanger. *J. Biol. Chem.* **1991**, *266*, 2739−2745.
(78) Eastman, P.; Swails, J.; Chodera, J. D.; McGibbon, R. T.; Zhao, Y.; Beauchamp, K. A.; Wang, L.-P.; Simmonett, A. C.; Harrigan, M. P.; Stern, C. D.; Wiewiora, R. P.; Brooks, B. R.; Pande, V. S. OpenMM 7: Rapid development of high performance algorithms for molecular dynamics. *PLOS Computational Biology* **2017**, *13*, No. e1005659.
(79) Maier, J. A.; Martinez, C.; Kasavajhala, K.; Wickstrom, L.; Hauser, K. E.; Simmerling, C. ff14SB: improving the accuracy of protein side chain and backbone parameters from ff99SB. *J. Chem. Theory Comput.* **2015**, *11*, 3696−3713.
(80) Wang, J.; Wolf, R. M.; Caldwell, J. W.; Kollman, P. A.; Case, D. A. Development and testing of a general amber force field. *Journal of computational chemistry* **2004**, *25*, 1157−1174.
(81) Hopkins, C. W.; Le Grand, S.; Walker, R. C.; Roitberg, A. E. Long-time-step molecular dynamics through hydrogen mass repartitioning. *J. Chem. Theory Comput.* **2015**, *11*, 1864−1874.
(82) York, D. M.; Darden, T. A.; Pedersen, L. G. The effect of long-range electrostatic interactions in simulations of macromolecular crystals: A comparison of the Ewald and truncated list methods. *J. Chem. Phys.* **1993**, *99*, 8345−8348.
(83) Husic, B. E.; Pande, V. S. Markov state models: From an art to a science. *J. Am. Chem. Soc.* **2018**, *140*, 2386−2396.
(84) Shukla, D.; Hernández, C. X.; Weber, J. K.; Pande, V. S. Markov State Models Provide Insights into Dynamic Modulation of Protein Function. *Acc. Chem. Res.* **2015**, *48*, 414−422.
(85) Chodera, J. D.; Noé, F. Markov state models of biomolecular conformational dynamics. *Curr. Opin. Struct. Biol.* **2014**, *25*, 135−144.
(86) Gu, S.; Silva, D.-A.; Meng, L.; Yue, A.; Huang, X. Quantitatively Characterizing the Ligand Binding Mechanisms of Choline Binding Protein Using Markov State Model Analysis. *PLoS Computational Biology* **2014**, *10*, No. e1003767.
(87) Moffett, A. S.; Shukla, D. Using molecular simulation to explore the nanoscale dynamics of the plant kinome. *Biochem. J.* **2018**, *475*, 905−921.
(88) Selvam, B.; Yu, Y.-C.; Chen, L.-Q.; Shukla, D. Molecular Basis of the Glucose Transport Mechanism in Plants. *ACS Central Science* **2019**, *5*, 1085−1096.
(89) Cheng, K. J.; Selvam, B.; Chen, L.-Q.; Shukla, D. Distinct substrate transport mechanism identified in homologous sugar transporters. *J. Phys. Chem. B* **2019**, *123*, 8411−8418.
(90) Feng, J.; Selvam, B.; Shukla, D. How do antiporters exchange substrates across the cell membrane? An atomic-level description of the complete exchange cycle in NarK. *Structure* **2021**, *29*, 922−933.e3.
(91) Chan, M. C.; Shukla, D. Markov state modeling of membrane transport proteins. *J. Struct. Biol.* **2021**, *213*, 107800.
(92) Scherer, M. K.; Trendelkamp-Schroer, B.; Paul, F.; Pérez-Hernández, G.; Hoffmann, M.; Plattner, N.; Wehmeyer, C.; Prinz, J.-H.; Noé, F. PyEMMA 2: A Software Package for Estimation, Validation, and Analysis of Markov Models. *J. Chem. Theory Comput.* **2015**, *11*, 5525−5542.
(93) Roe, D. R.; Cheatham, T. E. PTRAJ and CPPTRAJ: Software for Processing and Analysis of Molecular Dynamics Trajectory Data. *J. Chem. Theory Comput.* **2013**, *9*, 3084−3095.
(94) Humphrey, W.; Dalke, A.; Schulten, K. VMD: Visual molecular dynamics. *J. Mol. Graphics* **1996**, *14*, 33−38.

https://doi.org/10.1021/acschemneuro.1c00714
ACS Chem. Neurosci. 2022, 13, 933−945